Journal of Computational Electronics 4: 175–178, 2005

The Role of Long-Range Forces in Porin Channel Conduction

SHELA ABOUD
Electrical and Computer Engineering Department, Worcester Polytechnic Institute, Worcester, MA 01609
saboud@wpi.edu

DAVID MARREIRO AND MARCO SARANITI
Electrical and Computer Engineering Department, Illinois Institute of Technology, Chicago, IL 60616

ROBERT EISENBERG
Molecular Biophysics Department, Rush University, Chicago, IL 60612

Abstract. A fully self-consistent 3D Poisson P^3M Brownian dynamics solver is used to investigate the role of the long-range electrostatic forces on the selectivity and conductivity of OmpF porin. Our simulations show that even with zero applied bias, the long-range interactions are an important component of the total potential energy. In addition, the long-range force due to mobile carriers is shown to play a role in facilitating the flow of anions through the OmpF channel by screening the effect of the negative fixed charge of the protein.

Keywords: P^3M force field, Brownian dynamics, OmpF porin

1. Introduction

OmpF porin is a wide ion channel found in the outer membrane of *Escherichia coli* [1]. These proteins are considered passive transporters that function as ion channels with high conductivity and relatively low selectivity [2]. OmpF is a trimer, where each monomer is a hollow β-barrel structure with eight loops (L1-L8) that form the water-filled pore. Loop L3 folds inside the barrel and generates a physical constriction that reduces the lumen of the pore to a diameter of approximately 6 Ångstroms. In this constriction zone, the presence of two acidic residues (GLU-117 and ASP-113) on L3, and a cluster of three basic residues (ARG-42, ARG-82 and ARG-132) on the opposite wall of the pore, generates a large electrostatic potential. The cross-section of a single OmpF monomer (protein database code 2omf.pdb [3]) at the constriction zone is shown in Fig. 1, where the L3 loop and the charged residues are explicitly shown. The protonation state of the residues at neutral pH gives the OmpF porin channel an overall charge of $-30e$ [3] making it more cation selective [4]. In fact, while the cations can traverse the channel unaided, the permeation of an anion requires the presence of additional cations within the pore [5]. The selectivity of the porin channel also depends on the surrounding electrolyte solution, and increases with decreasing ionic concentrations. This fact has been attributed to a decrease in the electrostatic screening of the pore lining when less ions are present [4].

The wide range of experimental [6,7] and simulation [4,5,8] data available on porin channels make them a valuable stucture both for the investigation of the atomic details involved in ion transport, and as a benchmark for simulation methodologies. In this work, a Brownian dynamics (BD) simulation engine, self-consistently coupled to a 3D Poisson P^3M force field scheme [9] is used to investigate ionic flow in OmpF. BD approaches are attractive for modeling conductivity in porin because they represent a very good compromise between computational accuracy and efficiency. A crucial component of our simulation ap-

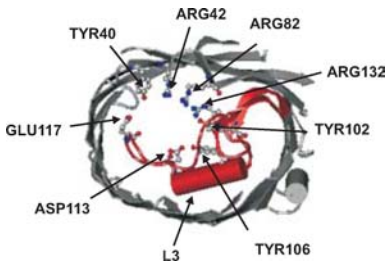

Figure 1. The constriction zone in one monomer of the OmpF porin. The L3 loop and the charged residues giving rise to the transverse electric field are explicitly shown.

proach is the force field scheme used to account for the electrostatic interactions in the system. This is particularly true for the long-range part of the interaction which sets the transmembrane potential that ultimately drives the ions into the channel. Furthermore, the use of a self-consistent force-field scheme that updates the solution of Poisson's equation at each time step, allows for the accurate inclusion of forces arising from the instantaneous distribution of charges in the system. The main goal of this study is to investigate the role of the pore charge distribution on the channel transport properties and examine the impact of the long-range forces on conduction.

A brief description of the BD algorithm will be given in the next section, followed by an overview of the method used to implement the self-consistent force-field scheme. An analysis of the potential energy profile inside the OmpF channel is then presented, and the impact of the long-range forces on the channel selectivity and conductivity is discussed.

2. P^3M Brownian Dynamics Solver

Within the P^3M-BD simulation approach, the porin is treated as a rigid structure embedded in a dielectric slab which represents the lipid bilayer. The channel/membrane system is surrounded by an electrolyte solution and the solvent is treated as a dielectric continuum. The trajectory of each ion in the electrolyte solution is described by the full Langevin equation [9], which is integrated using a third order scheme [10] that allows for a free-flight time step of 20 fs. A 3D Poisson P^3M algorithm [11,12] is used to calculate the electrostatic forces in the system. In particular, the long-range interaction that includes the external boundary conditions and the dielectric interfaces, is resolved with a 3D multigrid Poisson solver [13]. A triangular shaped cloud (third order) scheme [11] is used for both the charge assignment and the force interpolation. The short-range interaction between close particles is modeled in a small region surrounding each ion as a pure Coulomb term coupled to a Lennard-Jones potential [14] that represents the van der Waals interaction from overlapping molecular orbitals. Finally, a reference force is used to account for the double counting that arises from the geometric overlap of the long- and short-range domains [11].

3. Results and Discussion

The computational domain is discretized by a homogeneous $20 \times 20 \times 20$ tensor-product grid with a 1.0 nm mesh size in all three directions. Dirichlet boundary conditions are placed on the two planes perpendicular to the transport direction, while (reflecting) Neumann boundary conditions are imposed on the other 4 planes. The Dirichlet "contacts" are treated as open boundaries, and ions that traverse these regions exit from the simulation. The Dirichlet "contacts" are also used to maintain the initial concentration in the boundary layers by periodically injecting ions.

This computational approach has previously been successfully validated for the bulk electrolyte solution by comparing the radial distribution function calculated with the P^3M BD solver and an analytic model [9]. Another validation of the solver has been obtained by calculating the transmembrane potential, which provides the force that drives the ions into the channel. This test has been performed by running simulations of a 2 nm dielectric slab bathed by an electrolyte solution (no channel is present) under an externally imposed bias. Figure 2 shows the average anion and cation concentration along the direction perpendicular to the plane of the dielectric membrane (and to the Dirichlet boundaries) under an external bias of 1.0 V. A 0.3 M KCl concentration is set on one side of the slab, while 0.15 M is set on the other. As expected, the dielectric force gives rise to an increase (decrease) in the anion (cation) density on the left side of the dielectric membrane and a decrease (increase) in the anion (cation) density on the right side.

The atomic coordinates of the OmpF trimer obtained from the X-ray structure [3] are used to determine the fixed charge distribution with the Gromacs simulation package [15]. The standard protonation states of the residues at pH $=$ 7 are used [8,15], resulting in a

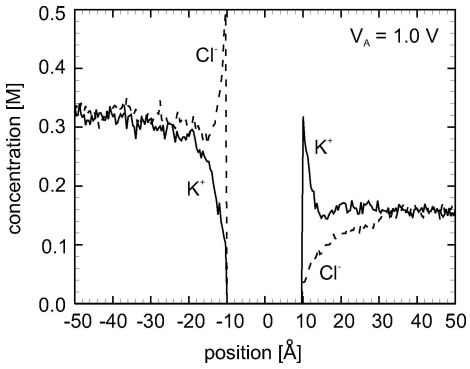

Figure 2. Average anion (Cl^-) and cation (K^+) concentration across a dielectric membrane with an extrenal bias of 1.0 V. The bulk concentration of KCl is 0.3 M on the left and 0.15 M on the right side of the central membrane.

total net charge of $-30e$ for the Ompf porin channel. Two bands of tyrosine molecules line the outer surface of the porin and anchor the protein to the lipid bilayer [16], the position of the ion channel within the dielectric slab is therefore determined by the location of the hydroxyl oxygen atoms of the tyrosine [4]. The thickness of the dielectric slab is 3 nm and a dielectric constant of 2 is used for both the slab and the protein, following the work of [5]. The porin/membrane system is oriented in the computational domain so that the charge flux through the channel will be perpendicular to the Dirichlet planes. To prevent ions inside the channel pore from penetrating the internal wall of the OmpF, which would be unphysical, an additional "core" repulsion is included in the force calculation for ions that come within a certain distant of the atoms in the protein wall [4,5]. In this work, this distance has been chosen to be the radius of K^+.

The electrostatic profile inside the OmpF channel is found by placing a probe ion throughout the trimer domain and calculating the corresponding potential energy. A minimum distance (equal to the ion radius) is enforced between the ion and the other charges in the system. A slice of the potential energy profile at the constriction zone under a zero external bias is shown in Fig. 3 for (a) a cation (K^+) with the full force-field scheme, (b) a cation (K^+) neglecting the long-range interaction, and (c) an anion (Cl^-) with the full force-field scheme. Superimposed over each contour plot is the OmpF molecular structure at the constriction. As can be seen, including the solution to Poisson's equation results in an lower potential energy even at zero bias. It should be noted that the calculation has not been corrected for the particle self-energy [17], but for

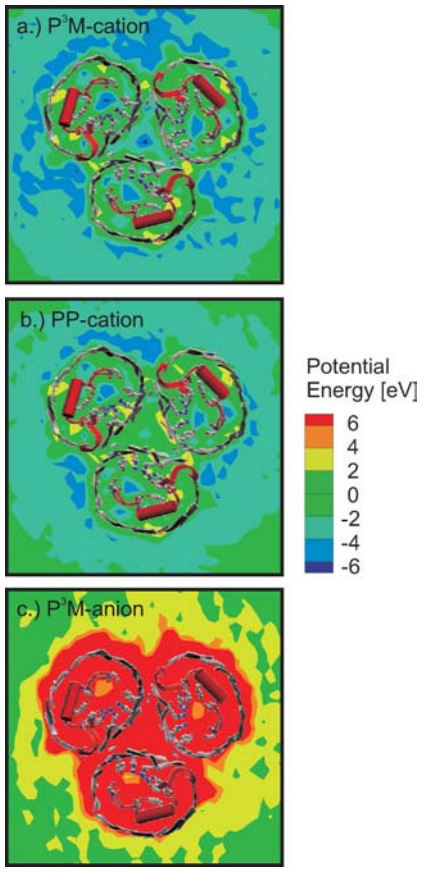

Figure 3. The potential energy profile felt by different ions with zero external bias. Plot (a) shows the total potential energy of a cation and plot (b) shows just the corresponding short-range contribution. Plot (c) is the total potential energy of an anion. The molecular structure of OmpF in the constriction zone is superimposed over the potential energy plots.

particles with the same self-energy its inclusion will not change the relative potential energy differences. As can been seen from the potential energy profile in Fig. 3(a), the cation experiences a potential that facilitates its flow into the channel, while the electrostatic barrier seen by the anion is very large (see Fig. 3(c)). Even when a large external bias is applied, the charged residues in the OmpF pin the potential energy, and the anions cannot flow through the constriction zone.

Since the flow of anions through OmpF was found by Im et al. [5] to be dependent on the presence of cations, the potential energy profile for an anion when a cation is placed in one of the OmpF pores is also calculated. The cation is placed at the position corresponding to its minimum potential energy in the constriction zone of one of the pores (which, for clarity, will be called pore

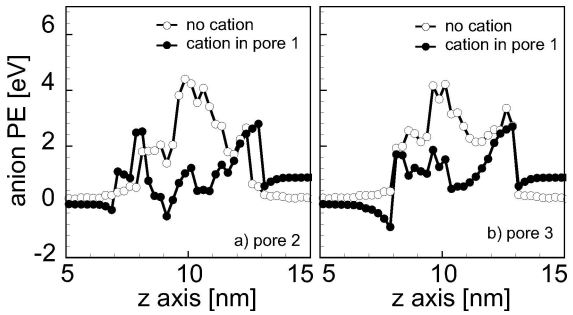

Figure 4. A comparison of the anion potential energy along the minimum energy pathway in (a) pore 2 and (b) pore 3 with and without a cation in pore 1.

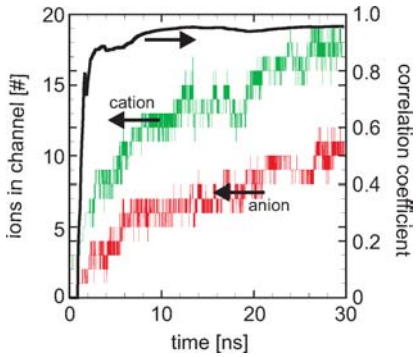

Figure 5. The number of anions and cations in the OmpF trimer as a function of time. The corresponding correlation coefficient is also shown.

(1) and the potential energy profile of the anion probe is calculated as described previously. As expected, the result is a significant decrease in the potential barrier seen by the anion as it enters pore 1. Interestingly, the presence of the cation in pore 1 also significantly changes the potential barrier seen by anions in the other two pores (pore 2 and 3). Figure 4 shows a comparison of the minimum potential energy pathway along (a) pore 2 and (b) pore 3, with and without a cation in pore 1. It can be seen that the addition of one positive charge in a neighboring pore significantly changes the potential energy profile of the anion in the other pores, making the entire OmpF less selective. This is also consistent with the experimental observation of decreasing selectivity with increasing ionic concentration [18], which is shown here for a single ion.

A plot is shown in Fig. 5 of the total number of K^+ and Cl^- ions inside the three pores of the OmpF channel as a function of time when the concentration of KCl is set to 0.1 M on either side of the membrane and an external bias of 1 V is applied. The entire domain is simulated for 30 ns. The correlation coefficient [19] of the number of anions and cations shows a strong correlation between ionic populations. While correlations between ions within a single OmpF monomer have been observed in other works [5,20], our simulations suggest that due to the long-range force, the correlation can span the protein and couple the transport of ions in all three pores.

References

1. J.M. Berg, J.L. Tymoczko, and L. Stryer, *Biochemistry* (W. H. Freeman and Company, 5th edition, 2001).
2. D.P. Tieleman, P.C. Bigging, G.R. Smith, and M.S.P. Sansom, *Quarterly Reviews of Biophysics*, **34**(4), 473 (2001).
3. A. Karshikoff, V. Spassov, S.W. Cowan, R. Ladenstein, and T. Schirmer, *Journal of Molecular Biology*, **240**, 372 (1994).
4. T. Schirmer and P. Phale, *Journal of Molecular Biology*, **294**, 1159 (1999).
5. W. Im and B. Roux, *Journal of Molecular Biology*, **319**(5), 1177 (2002).
6. P.S. Phale, A. Philippsen, C. Widmer, V.P. Phale, J.P. Rosenbusch, and T. Schirmer, *Biochemistry*, **40**(21), 6319 (2001).
7. E.M. Nestorovich, T.K. Rostovtseva, and S.M. Bezrukov, *Biophysical Journal*, **85**(6), 3718 (2003).
8. S. Varma and E. Jakobsson, *Biophysical Journal*, **86**(2), 690 (2004).
9. S. Aboud, M. Saraniti, and R. Eisenberg, *Journal of Computational Electronics*, (2004), accepted for publication.
10. W.F. van Gunsteren and H.J.C. Berendsen, *Molecular Physics*, **45**(3), 637 (1982).
11. R.W. Hockney and J.W. Eastwood, *Computer Simulation Using Particles* (Adam Hilger, Bristol, 1988).
12. C.J. Wordelman and U. Ravaioli, *IEEE Transaction on Electron Devices*, **47**(2), 410 (2000).
13. S.J. Wigger, M. Saraniti, and S.M. Goodnick, in *Proceedings of Second International Conference on Modeling and Simulation of Microsystems, MSM99*, Puerto Rico (PR), April 1999, p. 415.
14. R.S. Berry, S.A. Rice, and J. Ross, *Physical Chemistry*, (Oxford University Press, II edition, May 2000).
15. D. van der Spoel, A.R. van Buuren, E. Apol, P.J. Meulenhoff, D.P. Tieleman, A.L. T.M. Sijbers, B. Hess, K.A. Feenstra, E. Landahl, R. van Drunen, and H.J.C. Berendsen, Nijenborgh 4, 9747 AG Groningen, The Netherlands. Internet: http//www.gromacs.org, (2001).
16. D.P. Tieleman, L.R. Forrest, M. Sansom, and H.J.C. Berendsen, *Biochemistry*, **37**, 17554 (1998).
17. E.L. Pollock and J. Glosli, *Computer Physics Communications*, **95**, 93 (1996).
18. K.-L. Lou, N. Saint, A. Prilipov, G. Rummel, S.A. Benson, J.P. Rosenbusch, and T. Schirmer, *Journal of Biological Chemistry*, **271**(34), 20669 (1996).
19. D. Zwillinger, *Standard Mathematical Tables and Formulae* (CRC Press, 2003).
20. W. Im and B. Roux, *Journal of Molecular Biology*, **322**(4), 851 (2002).